

Cite as: Z. Zhang *et al.*, *Science* 10.1126/science.aan6814 (2017).

Robust epitaxial growth of two-dimensional heterostructures, multiheterostructures, and superlattices

Zhengwei Zhang,^{1*} Peng Chen,^{1,3*} Xidong Duan,^{1,†} Ketao Zang,² Jun Luo,² Xiangfeng Duan^{1,3,‡}

¹State Key Laboratory for Chemo/Biosensing and Chemometrics, College of Chemistry and Chemical Engineering, Hunan University, Changsha 410082, China. ²Center for Electron Microscopy, Institute for New Energy Materials and Low-Carbon Technologies, School of Materials, Tianjin University of Technology, Tianjin 300384, China.

³Department of Chemistry and Biochemistry and California Nanosystems Institute, University of California, Los Angeles, CA 90095, USA.

*These authors contributed equally to this work.

†Corresponding author: E-mail: xidongduan@hnu.edu.cn; xduan@chem.ucla.edu

We report a general synthetic strategy for highly robust growth of diverse heterostructures, multiheterostructures, and superlattices from two-dimensional (2D) atomic crystals. A reverse flow during the temperature swing stage in sequential vapor deposition growth process allowed us to cool the existing 2D crystals to prevent undesired thermal degradation and uncontrolled homogeneous nucleation, thus enabling highly robust block-by-block epitaxial growth. Raman and photoluminescence mapping studies showed that a wide range of 2D heterostructures (such as WS₂-WSe₂ and WS₂-MoSe₂), multiheterostructures (such as WS₂-WSe₂-MoS₂ and WS₂-MoSe₂-WSe₂), and superlattices (such as WS₂-WSe₂-WS₂-WSe₂-WS₂) were readily prepared with precisely controlled spatial-modulation. Transmission electron microscope studies show clear chemical modulation with atomically sharp interfaces. Electrical transport studies of WSe₂-WS₂ lateral junctions show well-defined diode characteristics with a rectification ratio up to 10⁵.

The two-dimensional (2D) atomic crystals of transition metal dichalcogenides (TMDs) (*e.g.*, MoS₂, MoSe₂, WS₂ and WSe₂) have attracted intense recent interest (*I–II*). To explore the full potential of these 2D atomic crystals requires reliable synthesis of their heterostructures and superlattices with precisely defined spatial modulation of chemical compositions and electronic structures. Despite considerable efforts and some successful examples to date (*I2–21*), the robust synthesis of the atomically thin 2D TMD heterostructures remains a significant challenge and the epitaxial growth of 2D superlattices with multiple alternating blocks has not been realized.

To date, diverse monolayer atomic crystals as well as their alloys have been successfully grown via chemical vapor deposition (CVD) or thermal CVD process by using various chemical vapor sources (*22–33*). With a similar crystal structure and comparable lattice constants among these 2D crystals, in-domain lateral heterostructures have also been successfully synthesized through a two-step epitaxial growth of a second material (*e.g.*, MoSe₂, WSe₂) at the edge of an existing domain of a first material (*e.g.*, MoS₂, WS₂) (*I2–21*). In principle, such sequential growth process can be repeated multiple times for the block-by-block growth of multiheterostructures (with multiple distinct material blocks) or superlattices (with multiple alternating blocks) by switching the chemical vapor source or modulating the exact growth conditions in each growth steps.

To rationally produce lateral heterostructures with mul-

tiple distinct material blocks requires sequential growth steps with different chemical supply, growth conditions, or both. The monolayer 2D crystals are usually too delicate to survive multiple sequential growth steps necessary for the formation of 2D heterostructures or superlattices. With just a single or a few atomic layers, the 2D crystals essentially have little tolerance for any thermal-induced degradation, and are more challenging to grow than other bulk or nanoscale heterostructures with more atomic layers. Additionally, the ill-controlled supply of chemical vapor sources during the temperature swing stage between the sequential growth steps often leads to undesired homogeneous nucleation. To experimentally realize robust step-by-step growth of atomically thin 2D heterostructures or superlattices, at least two key requirements must be satisfied. First, the nucleating block must be robust enough to survive the temperature or chemical environment swing between the sequential growth steps. Second, undesired homogeneous nucleation of the new crystal seeds must be minimized and ensure exclusive heterogeneous epitaxial growth at the edge of the existing 2D crystals.

Although the growth of 2D heterostructures has been demonstrated, the studies to date are largely limited to the simplest heterostructures with only two distinct material blocks for a few selected material combinations. The growth of multiheterostructures or superlattices with three or more distinct material blocks, which requires sequential growth with multiple back-and-forth swings between the less and

more aggressive synthetic conditions, making it inevitable that existing blocks are damaged when the subsequent growth step is carried out in a more aggressive condition (*e.g.*, higher temperature) than the prior step.

We designed a modified step-by-step thermal CVD process in which a selected source powder is heated and vaporized under a flow of argon carrier gas for each sequential step, and the heterostructures are formed by the continued lateral epitaxial growth at the edge of the first monolayer crystals placed at the downstream end of CVD furnace [See more details of modified growth process in the supplementary materials (34)]. In a typical sequential growth process, the excessive thermal degradation (fig. S1) or uncontrolled nucleation (fig. S2) during the temperature swing between sequential growth steps represents the key obstacles to reliable formation of monolayer heterostructures. To avoid such adverse effects, we used a reverse flow from the substrate to the source during the temperature swing between successive growth steps (Fig. 1A). A forward flow from chemical vapor source was only applied at the exact growth temperature. With such reverse flow, the existing monolayer materials on the growth substrate were continuously flushed by the cold argon gas during the temperature swing to reduce exposure to high temperature and minimize thermal degradation. The reverse flow from the substrate to the source during the temperature ramping-up stage could also prevent unintended supply of chemical vapor source at undesired temperature to eliminate uncontrolled homogeneous nucleation. With a high degree of controllability in each step, the integrity and quality of monolayer heterostructures can be well preserved after multiple sequential growth steps. This approach can thus offer a general and reliable strategy for the growth of a wide range of heterostructures, multiheterostructures and superlattices (Fig. 1B-E, fig. S3).

We used our approach initially for the general synthesis a wide range of 2D crystal heterostructures. Figure 2A₁ shows the optical microscope image of a synthesized triangular domain of WS₂-WSe₂ monolayer heterostructure on SiO₂/Si substrate, which exhibits two concentric regions with slightly different optical contrast. Atomic force microscope (AFM) studies show that the heterostructure domain exhibits a smooth surface with a single step-height of 0.75 nm (fig. S4), confirming the monolayer nature of the heterostructure domain. To probe the spatial modulation of the structural and optical properties in the resulting WS₂-WSe₂ heterostructures, we have conducted micro-Raman and micro-photoluminescence (micro-PL) studies using a confocal Raman microscope. The Raman spectra taken from the center and peripheral regions of the triangular domain clearly show distinct features. The Raman spectrum from the center region exhibit two prominent peak at 350 cm⁻¹ and 419 cm⁻¹ (pink line in Fig. 2A₂), corresponding to the E' and A_{1'}

resonance modes of WS₂; while the Raman spectrum from the peripheral region display one prominent peak at 250 cm⁻¹ (green line in Fig. 2A₂), in agreement of the A_{1'} resonance modes of WSe₂, respectively (35, 36). These micro-Raman studies demonstrate the co-existence of two distinct materials within the same triangular domain. The spatially resolved Raman mapping studies further reveals the spatial modulation within the triangular domain, with the center part consisting of a triangular domain of WS₂ and the peripheral region composed of WSe₂ (Fig. 2A₃)

Similarly, micro-PL studies also show highly distinct photoluminescence peaks at 630 nm for the center part and 760 nm for the peripheral part (Fig. 2A₄), consistent with the near band-edge emission from WS₂ and WSe₂, respectively (36, 37). The PL mapping studies (Fig. 2A₅-2A₆) show features similar to those of Raman mapping studies, further confirming the formation of WS₂-WSe₂ lateral heterostructures. The PL spectra at the interface region display two distinct peaks (fig. S5A) with the peak positions displaying little deviation from those of the center region (WS₂) or the peripheral region (WSe₂). The simple overlap of the PL spectra at interface indicates rather sharp transition from WS₂ to WSe₂ at the interface of the synthesized lateral heterostructure (13), as will be further evidenced below. Using the same strategy, we synthesized a wide range of monolayer heterostructures including WSe₂-MoS₂ (Fig. 2B₁-B₃), WS₂-MoS₂ (Fig. 2C₁-C₃), WSe₂-MoSe₂ (Fig. 2D₁-D₃), and WS₂-MoSe₂ (Fig. 2E₁-E₃), which as shown by optical microscopy, Raman spectroscopy and PL mapping studies (fig. S6), formed lateral heterojunctions similar to the WS₂-WSe₂ heterostructures.

We also grew more complex compositionally modulated superlattices or multiheterostructures through a step-by-step growth process, in which the number of periods and repeating spacing can be readily varied during growth. The optical microscope image of a synthesized WS₂-WSe₂-WS₂-WSe₂ monolayer superlattice on SiO₂/Si substrate (Fig. 3A₁) exhibited four concentric regions with slightly different optical contrast. The spatially resolved Raman mapping at 350 cm⁻¹ (E' mode of WS₂) and 250 cm⁻¹ (A_{1'} mode of WSe₂) (Fig. 3A₂) revealed the spatial modulation of the triangular domain: with the first and third parts composed of WS₂ and the second and fourth parts composed of WSe₂. Thus, a seamless lateral superlattice structure formed within the same triangular domain. The PL mapping images at 630 nm (near band edge emission of WS₂; Fig. 3A₃) and 760 nm (near band edge emission band edge of WSe₂; Fig. 3A₄) also confirmed the formation of WS₂-WSe₂ monolayer lateral superlattice structure. In addition to the lateral superlattices, monolayer lateral multiheterostructures including WS₂-MoS₂-WS₂, WS₂-WSe₂-MoS₂ and WS₂-MoSe₂-WSe₂ were synthesized, and optical microscopy, Raman and PL characteri-

zations of these lateral multiheterostructures confirmed the formation of multiheterostructures with well-defined spatial modulation (Fig. 3B₁-D₅).

The detailed atomic structure of the lateral heterostructure interface was revealed by high-angle annular dark-field scanning transmission electron microscope (HAADF-STEM) Z-contrast imaging. Figure 4A shows a Z-contrast image of the WS₂-WSe₂ lateral interface, where Se atoms exhibit higher image intensity than the S atoms. The atomically sharp interface can be clearly observed along the overall-straight “interline” in the WS₂-WSe₂ lateral junction. The WS₂ and WSe₂ domains connect seamlessly at the interface into a single hexagonal monolayer lattice and share the same crystal orientation. The corresponding atomic model, obtained via atom-by-atom image quantification indicates the seamless connection and atomically abrupt transition between the WS₂ and WSe₂ lattice. Figure 4B further showed the atomic structure of WS₂-MoSe₂ lateral junction, where an atomically sharp “interline” was also well resolved.

We further investigated the structural modulation across the WS₂-MoSe₂-WSe₂ multi-heterostructure using the low-magnification Z-contrast image. Three regions with slightly different contrast were observed, corresponding to the WS₂, MoSe₂ and WSe₂, respectively. The selected area electron diffraction (SAED) patterns are taken at the WS₂ region, MoSe₂ region and WSe₂ region, respectively (Fig. 4, D-F). The hexagonally arranged diffraction spots can be indexed to the hexagonal symmetry of the [001] zone plane of WS₂, MoSe₂ and WSe₂ lattice structures. A careful analysis of these diffraction peaks yields (100) lattice plane spacings of 2.70 Å, 2.77 Å and 2.81 Å, in agreement with the values for WS₂, MoSe₂ and WSe₂ (12, 38). Figure 4G-I show the high-resolution STEM images of WS₂, MoSe₂ and WSe₂. Based on these images, we can also determine the (100) lattice plane spacings of WS₂, MoSe₂ and WSe₂ to be 2.70 Å, 2.79 Å and 2.81 Å, consistent with the lattice plane spacings yielded from SAED studies. Together, these studies demonstrate the well-defined chemical/structural modulation in 2D crystal heterostructures and multi-heterostructures with atomically sharp interfaces.

With the atomically sharp interface, the width of heteroepitaxy can be controlled down to nanometer scale (fig. S7), which may enable the realization of ultrashort period superlattices or and open up a pathway to multi-quantum-well (or “quantum-line”) structure in the 2D atomic crystals. To further characterize the electronic properties of the monolayer heterostructures, we have also fabricated the monolayer lateral p-n junction device from WSe₂-WS₂ lateral heterostructures by taking advantage of the intrinsically p-type characteristics of WSe₂ and the n-type characteristics of WS₂. The current versus voltage measurements showed a rectification ratio up to 10⁵ (fig. S8), consistent with the

presence of a monolayer lateral p-n junction. The robust synthesis of diverse 2D heterostructures and superlattices with atomically sharp interfaces creates an interesting material system for fundamental studies and novel device demonstrations at the limit of single atomic thickness, which will be an important topic for future studies. Furthermore, by using site specific nucleating blocks obtained from lithography patterning or patterned growth (39), a similar sequential epitaxial growth may be used for producing complex heterostructures with controlled location and orientation, which will be important for developing practical technologies from these atomically thin crystals.

REFERENCES AND NOTES

1. K. S. Novoselov, D. Jiang, F. Schedin, T. J. Booth, V. V. Khotkevich, S. V. Morozov, A. K. Geim, Two-dimensional atomic crystals. *Proc. Natl. Acad. Sci. U.S.A.* **102**, 10451–10453 (2005). doi:[10.1073/pnas.0502848102](https://doi.org/10.1073/pnas.0502848102) Medline
2. Q. H. Wang, K. Kalantar-Zadeh, A. Kis, J. N. Coleman, M. S. Strano, Electronics and optoelectronics of two-dimensional transition metal dichalcogenides. *Nat. Nanotechnol.* **7**, 699–712 (2012). doi:[10.1038/nnano.2012.193](https://doi.org/10.1038/nnano.2012.193) Medline
3. A. M. Jones, H. Yu, J. S. Ross, P. Klement, N. J. Ghimire, J. Yan, D. G. Mandrus, W. Yao, X. Xu, Spin-layer locking effects in optical orientation of exciton spin in bilayer WSe₂. *Nat. Phys.* **10**, 130–134 (2014). doi:[10.1038/nphys2848](https://doi.org/10.1038/nphys2848)
4. A. Pospischil, M. M. Furchi, T. Mueller, Solar-energy conversion and light emission in an atomic monolayer p-n diode. *Nat. Nanotechnol.* **9**, 257–261 (2014). doi:[10.1038/nnano.2014.14](https://doi.org/10.1038/nnano.2014.14) Medline
5. C.-H. Lee, G.-H. Lee, A. M. van der Zande, W. Chen, Y. Li, M. Han, X. Cui, G. Arefe, C. Nuckolls, T. F. Heinz, J. Guo, J. Hone, P. Kim, Atomically thin p-n junctions with van der Waals heterointerfaces. *Nat. Nanotechnol.* **9**, 676–681 (2014). doi:[10.1038/nnano.2014.150](https://doi.org/10.1038/nnano.2014.150) Medline
6. W. J. Yu, Z. Li, H. Zhou, Y. Chen, Y. Wang, Y. Huang, X. Duan, Vertically stacked multi-heterostructures of layered materials for logic transistors and complementary inverters. *Nat. Mater.* **12**, 246–252 (2013). doi:[10.1038/nmat3518](https://doi.org/10.1038/nmat3518) Medline
7. B. W. H. Baugher, H. O. H. Churchill, Y. Yang, P. Jarillo-Herrero, Optoelectronic devices based on electrically tunable p-n diodes in a monolayer dichalcogenide. *Nat. Nanotechnol.* **9**, 262–267 (2014). doi:[10.1038/nnano.2014.25](https://doi.org/10.1038/nnano.2014.25) Medline
8. W. J. Yu, Y. Liu, H. Zhou, A. Yin, Z. Li, Y. Huang, X. Duan, Highly efficient gate-tunable photocurrent generation in vertical heterostructures of layered materials. *Nat. Nanotechnol.* **8**, 952–958 (2013). doi:[10.1038/nnano.2013.219](https://doi.org/10.1038/nnano.2013.219) Medline
9. P. Rivera, K. L. Seyler, H. Yu, J. R. Schaibley, J. Yan, D. G. Mandrus, W. Yao, X. Xu, Valley-polarized exciton dynamics in a 2D semiconductor heterostructure. *Science* **351**, 688–691 (2016). doi:[10.1126/science.aac7820](https://doi.org/10.1126/science.aac7820) Medline
10. S. Wu, S. Buckley, J. R. Schaibley, L. Feng, J. Yan, D. G. Mandrus, F. Hatami, W. Yao, J. Vučković, A. Majumdar, X. Xu, Monolayer semiconductor nanocavity lasers with ultralow thresholds. *Nature* **520**, 69–72 (2015). doi:[10.1038/nature14290](https://doi.org/10.1038/nature14290) Medline
11. S. B. Desai, S. R. Madhvapathy, A. B. Sachid, J. P. Llinas, Q. Wang, G. H. Ahn, G. Pitner, M. J. Kim, J. Bokor, C. Hu, H. P. Wong, A. Javey, MoS₂ transistors with 1-nanometer gate lengths. *Science* **354**, 99–102 (2016). doi:[10.1126/science.aaa4698](https://doi.org/10.1126/science.aaa4698) Medline
12. X. Duan, C. Wang, J. C. Shaw, R. Cheng, Y. Chen, H. Li, X. Wu, Y. Tang, Q. Zhang, A. Pan, J. Jiang, R. Yu, Y. Huang, X. Duan, Lateral epitaxial growth of two-dimensional layered semiconductor heterojunctions. *Nat. Nanotechnol.* **9**, 1024–1030 (2014). doi:[10.1038/nnano.2014.222](https://doi.org/10.1038/nnano.2014.222) Medline
13. M.-Y. Li, Y. Shi, C.-C. Cheng, L.-S. Lu, Y.-C. Lin, H.-L. Tang, M.-L. Tsai, C.-W. Chu, K.-H. Wei, J.-H. He, W.-H. Chang, K. Suenaga, L.-J. Li, Epitaxial growth of a monolayer WSe₂-MoS₂ lateral p-n junction with an atomically sharp interface. *Science* **349**, 524–528 (2015). doi:[10.1126/science.aab4097](https://doi.org/10.1126/science.aab4097) Medline
14. Y. Gong, J. Lin, X. Wang, G. Shi, S. Lei, Z. Lin, X. Zou, G. Ye, R. Vajtai, B. I. Yakobson, H. Terrones, M. Terrones, B. K. Tay, J. Lou, S. T. Pantelides, Z. Liu, W. Zhou, P. M. Ajayan, Vertical and in-plane heterostructures from WS₂/MoS₂

- monolayers. *Nat. Mater.* **13**, 1135–1142 (2014). doi:[10.1038/nmat4091](https://doi.org/10.1038/nmat4091) Medline
15. C. Huang, S. Wu, A. M. Sanchez, J. J. P. Peters, R. Bearland, J. S. Ross, P. Rivera, W. Yao, D. H. Cobden, X. Xu, Lateral heterojunctions within monolayer MoSe₂-WS₂ semiconductors. *Nat. Mater.* **13**, 1096–1101 (2014). doi:[10.1038/nmat4064](https://doi.org/10.1038/nmat4064) Medline
 16. Y. Yoo, Z. P. Degregorio, J. E. Johns, Seed crystal homogeneity controls lateral and vertical heteroepitaxy of monolayer MoS₂ and WS₂. *J. Am. Chem. Soc.* **137**, 14281–14287 (2015). doi:[10.1021/jacs.5b06643](https://doi.org/10.1021/jacs.5b06643) Medline
 17. M. Mahjouri-Samani, M.-W. Lin, K. Wang, A. R. Lupini, J. Lee, L. Basile, A. Boulesbaa, C. M. Rouleau, A. A. Puretzky, I. N. Ivanov, K. Xiao, M. Yoon, D. B. Geohegan, Patterned arrays of lateral heterojunctions within monolayer two-dimensional semiconductors. *Nat. Commun.* **6**, 7749 (2015). doi:[10.1038/ncomms8749](https://doi.org/10.1038/ncomms8749) Medline
 18. C. Tan, H. Zhang, Epitaxial growth of hetero-nanostructures based on ultrathin two-dimensional nanosheets. *J. Am. Chem. Soc.* **137**, 12162–12174 (2015). doi:[10.1021/jacs.5b03590](https://doi.org/10.1021/jacs.5b03590) Medline
 19. K. Chen, X. Wan, J. Wen, W. Xie, Z. Kang, X. Zeng, H. Chen, J.-B. Xu, Electronic properties of MoS₂-WS₂ heterostructures synthesized with two-step lateral epitaxial strategy. *ACS Nano* **9**, 9868–9876 (2015). doi:[10.1021/acsnano.5b03188](https://doi.org/10.1021/acsnano.5b03188) Medline
 20. X.-Q. Zhang, C.-H. Lin, Y.-W. Tseng, K.-H. Huang, Y.-H. Lee, Synthesis of lateral heterostructures of semiconducting atomic layers. *Nano Lett.* **15**, 410–415 (2015). doi:[10.1021/nl503744f](https://doi.org/10.1021/nl503744f) Medline
 21. J. Chen, W. Zhou, W. Tang, B. Tian, X. Zhao, H. Xu, Y. Liu, D. Geng, S. J. R. Tan, W. Fu, K. P. Loh, Lateral epitaxy of atomically sharp WSe₂/WS₂ heterojunctions on silicon dioxide substrates. *Chem. Mater.* **28**, 7194–7197 (2016). doi:[10.1021/acs.chemmater.6b03639](https://doi.org/10.1021/acs.chemmater.6b03639)
 22. K.-K. Liu, W. Zhang, Y.-H. Lee, Y.-C. Lin, M.-T. Chang, C.-Y. Su, C.-S. Chang, H. Li, Y. Shi, H. Zhang, C.-S. Lai, L.-J. Li, Growth of large-area and highly crystalline MoS₂ thin layers on insulating substrates. *Nano Lett.* **12**, 1538–1544 (2012). doi:[10.1021/nl2043612](https://doi.org/10.1021/nl2043612) Medline
 23. Y.-H. Lee, X.-Q. Zhang, W. Zhang, M.-T. Chang, C.-T. Lin, K.-D. Chang, Y.-C. Yu, J. T.-W. Wang, C.-S. Chang, L.-J. Li, T.-W. Lin, Synthesis of large-area MoS₂ atomic layers with chemical vapor deposition. *Adv. Mater.* **24**, 2320–2325 (2012). doi:[10.1002/adma.201104798](https://doi.org/10.1002/adma.201104798) Medline
 24. K. Kang, S. Xie, L. Huang, Y. Han, P. Y. Huang, K. F. Mak, C.-J. Kim, D. Muller, J. Park, High-mobility three-atom-thick semiconducting films with wafer-scale homogeneity. *Nature* **520**, 656–660 (2015). doi:[10.1038/nature14417](https://doi.org/10.1038/nature14417) Medline
 25. Y.-H. Lee, L. Yu, H. Wang, W. Fang, X. Ling, Y. Shi, C.-T. Lin, J.-K. Huang, M.-T. Chang, C.-S. Chang, M. Dresselhaus, T. Palacios, L.-J. Li, J. Kong, Synthesis and transfer of single-layer transition metal disulfides on diverse surfaces. *Nano Lett.* **13**, 1852–1857 (2013). doi:[10.1021/nl400687n](https://doi.org/10.1021/nl400687n) Medline
 26. A. M. van der Zande, P. Y. Huang, D. A. Chenet, T. C. Berkelbach, Y. You, G.-H. Lee, T. F. Heinz, D. R. Reichman, D. A. Muller, J. C. Hone, Grains and grain boundaries in highly crystalline monolayer molybdenum disulphide. *Nat. Mater.* **12**, 554–561 (2013). doi:[10.1038/nmat3633](https://doi.org/10.1038/nmat3633) Medline
 27. M. Zhao, Y. Ye, Y. Han, Y. Xia, H. Zhu, S. Wang, Y. Wang, D. A. Muller, X. Zhang, Large-scale chemical assembly of atomically thin transistors and circuits. *Nat. Nanotechnol.* **11**, 954–959 (2016). doi:[10.1038/nnano.2016.115](https://doi.org/10.1038/nnano.2016.115) Medline
 28. Y. Zhang, Y. Zhang, Q. Ji, J. Ju, H. Yuan, J. Shi, T. Gao, D. Ma, M. Liu, Y. Chen, X. Song, H. Y. Hwang, Y. Cui, Z. Liu, Controlled growth of high-quality monolayer WS₂ layers on sapphire and imaging its grain boundary. *ACS Nano* **7**, 8963–8971 (2013). doi:[10.1021/nn403454e](https://doi.org/10.1021/nn403454e) Medline
 29. X. Wang, Y. Gong, G. Shi, W. L. Chow, K. Keyshar, G. Ye, R. Vajtai, J. Lou, Z. Liu, E. Ringe, B. K. Tay, P. M. Ajayan, Chemical vapor deposition growth of crystalline monolayer MoSe₂. *ACS Nano* **8**, 5125–5131 (2014). doi:[10.1021/nn501175k](https://doi.org/10.1021/nn501175k) Medline
 30. J. Mann, Q. Ma, P. M. Odenthal, M. Isarraraz, D. Le, E. Preciado, D. Barroso, K. Yamaguchi, G. von Son Palacio, A. Nguyen, T. Tran, M. Wurch, A. Nguyen, V. Klee, S. Bobek, D. Sun, T. F. Heinz, T. S. Rahman, R. Kawakami, L. Bartels, 2-dimensional transition metal dichalcogenides with tunable direct band gaps: MoS_{2(1-x)} Se_{2x} monolayers. *Adv. Mater.* **26**, 1399–1404 (2014). doi:[10.1002/adma.201304389](https://doi.org/10.1002/adma.201304389) Medline
 31. X. Lu, M. I. B. Utama, J. Lin, X. Gong, J. Zhang, Y. Zhao, S. T. Pantelides, J. Wang, Z. Dong, Z. Liu, W. Zhou, Q. Xiong, Large-area synthesis of monolayer and few-layer MoSe₂ films on SiO₂ substrates. *Nano Lett.* **14**, 2419–2425 (2014). doi:[10.1021/nl5000906](https://doi.org/10.1021/nl5000906) Medline
 32. H. Li, X. Duan, X. Wu, X. Zhuang, H. Zhou, Q. Zhang, X. Zhu, W. Hu, P. Ren, P. Guo, L. Ma, X. Fan, X. Wang, J. Xu, A. Pan, X. Duan, Growth of alloy MoS_(2-x)Se_{2(1-x)} nanosheets with fully tunable chemical compositions and optical properties. *J. Am. Chem. Soc.* **136**, 3756–3759 (2014). doi:[10.1021/ja500069b](https://doi.org/10.1021/ja500069b) Medline
 33. S. Tongay, D. S. Narang, J. Kang, W. Fan, C. Ko, A. V. Luce, K. X. Wang, J. Suh, K. D. Patel, V. M. Pathak, J. Li, J. Wu, Two-dimensional semiconductor alloys: Monolayer Mo_{1-x}W_xSe₂. *Appl. Phys. Lett.* **104**, 012101 (2014). doi:[10.1063/1.4834358](https://doi.org/10.1063/1.4834358)
 34. Supplementary materials are available on *Science* online.
 35. W. Zhao, Z. Ghorannevis, K. K. Amara, J. R. Pang, M. Toh, X. Zhang, C. Kloc, P. H. Tan, G. Eda, Lattice dynamics in mono- and few-layer sheets of WS₂ and WSe₂. *Nanoscale* **5**, 9677–9683 (2013). doi:[10.1039/c3nr03052k](https://doi.org/10.1039/c3nr03052k) Medline
 36. H. R. Gutierrez, N. Perea-Lopez, A. L. Elas, A. Berkdemir, B. Wang, R. Lv, F. Lopez-Urías, V. H. Crespi, H. Terrones, M. Terrones, Extraordinary room-temperature photoluminescence in triangular WS₂ monolayers. *Nano Lett.* **13**, 3447–3454 (2013). doi:[10.1021/nl3026357](https://doi.org/10.1021/nl3026357) Medline
 37. H. Sahin, S. Tongay, S. Horzum, W. Fan, J. Zhou, J. Li, J. Wu, F. M. Peeters, Anomalous Raman spectra and thickness-dependent electronic properties of WSe₂. *Phys. Rev. B Condens. Matter* **87**, 165409 (2013). doi:[10.1103/PhysRevB.87.165409](https://doi.org/10.1103/PhysRevB.87.165409)
 38. R. Coehoorn, C. Haas, J. Dijkstra, C. J. F. Flipse, R. A. de Groot, A. Wold, Electronic structure of MoSe₂, MoS₂, and WSe₂. I. Band-structure calculations and photoelectron spectroscopy. *Phys. Rev. B* **35**, 6195–6202 (1987). doi:[10.1103/PhysRevB.35.6195](https://doi.org/10.1103/PhysRevB.35.6195) Medline
 39. Y. Zhou, Y. Nie, Y. Liu, K. Yan, J. Hong, C. Jin, Y. Zhou, J. Yin, Z. Liu, H. Peng, Epitaxy and photoresponse of two-dimensional GaSe crystals on flexible transparent mica sheets. *ACS Nano* **8**, 1485–1490 (2014). doi:[10.1021/nn405529r](https://doi.org/10.1021/nn405529r) Medline

ACKNOWLEDGMENTS

We acknowledge the support from National Natural Science Foundation of China (No. 61528403). J.L. acknowledges support by National Program for Thousand Young Talents of China, Tianjin Municipal Science and Technology Commission (15JCYBJC52600), and Tianjin Municipal Education Commission. X.D. acknowledges the support by National Science Foundation DMR1508144. All data are reported in the main text and supplementary materials.

SUPPLEMENTARY MATERIALS

www.sciencemag.org/cgi/content/full/science.xxxxxx/DC1

Materials and Methods

Supplementary Text

Figs. S1 to S8

Table S1

18 May 2017; accepted 19 July 2017

Published online 3 August 2017

10.1126/science.aan6814

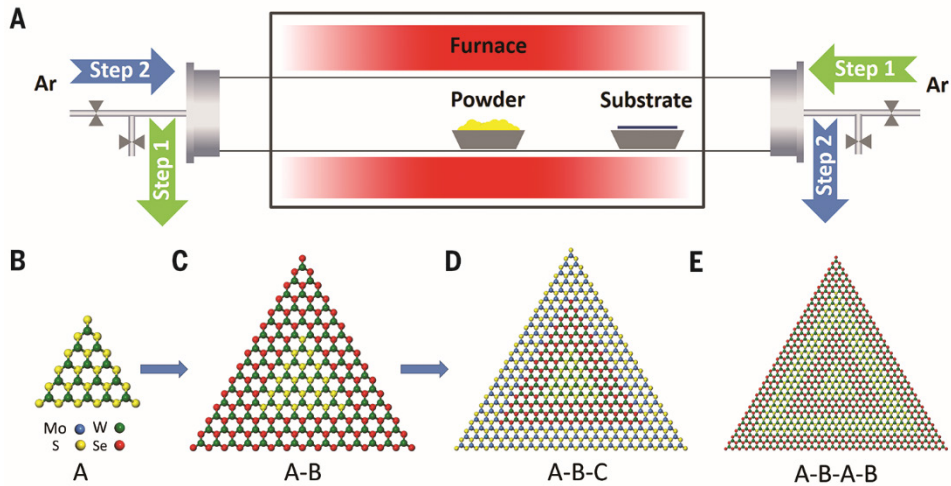


Fig. 1. Robust epitaxial growth of 2D monolayer heterostructures, multiheterostructures and superlattices with a modified CVD process. (A) Schematic illustration of a modified CVD system for the robust epitaxial growth of lateral heterostructures. The solid powders were directly used as the source material. Both sides of quartz tube are equipped with gas inlet and outlet. The direction of argon gas flow can be switched by using the angle-style valves at the two ends of quartz tube. A reverse flow from the substrate to the source is applied during the temperature ramping and stabilization stage to cool existing 2D crystal on substrate and prevent unintended supply of vapor source reactant or uncontrolled nucleation and growth (step 1). After reaching the desired growth temperature, a forward flow from the source to the substrate is applied to transport the vapor phase reactant onto the growth substrate for the epitaxial growth of the desired 2D crystals (step 2). The reverse flow can effectively prevent the unintended homogeneous nucleation and minimize the thermal degradation of the atomically thin 2D crystals to ensure highly robust sequential growth of (B) monolayer seed A, (C) A-B heterostructure, (D) A-B-C multiheterostructures, and (E) A-B-A-B superlattices.

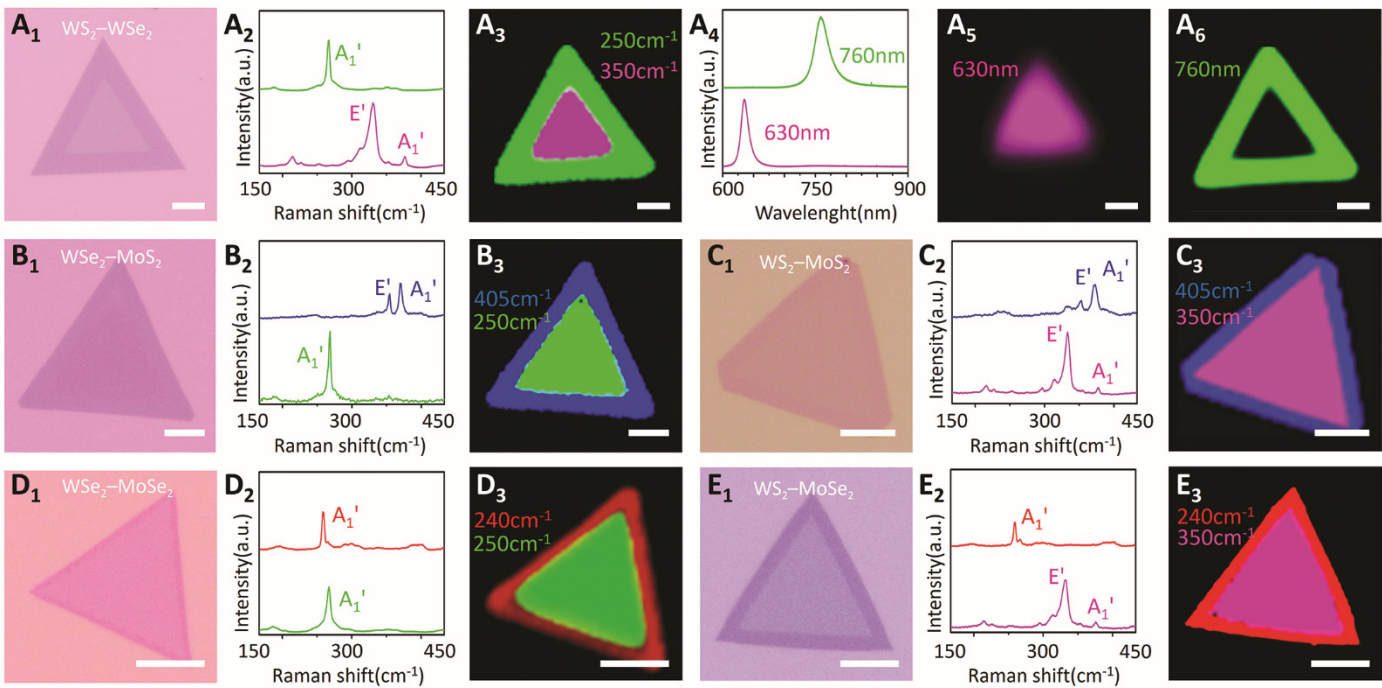


Fig. 2. General growth of diverse 2D lateral heterostructures. (A₁) Optical microscope image of a WS₂-WSe₂ heterostructure domain. (A₂) Raman spectra of the WS₂-WSe₂ heterostructure. The pink curve is obtained from the center region, showing the characteristic Raman peaks of WS₂; and the green curve is obtained from the peripheral region, showing the characteristic Raman peaks of WSe₂. (A₃) Spatially-resolved Raman mapping image shows clear lateral integration of the WS₂-WSe₂ heterostructure. (A₄) Photoluminescence (PL) spectra of the WS₂-WSe₂ heterostructure. The pink curve is obtained from the center region, showing the characteristic PL peak of WS₂; and the green curve is obtained from the peripheral region, showing the characteristic PL peak of WSe₂. (A₅-A₆) Spatially resolved PL mapping images at 630 nm and 760 nm, showing characteristic PL emission of WS₂ and WSe₂ in the center and peripheral regions of the triangular domain. (B₁-B₃) Optical microscope image, Raman spectra and mapping image of monolayer WSe₂-MoS₂ heterostructure. (C₁-C₃) Optical microscope image, Raman mapping spectra and image of monolayer WS₂-MoS₂ heterostructure. (D₁-D₃) Optical microscope image, Raman spectra and mapping image of monolayer WSe₂-MoSe₂ heterostructure. (E₁-E₃) Optical microscope image, Raman spectra and mapping image of monolayer WS₂-MoSe₂ heterostructure. All scale bars are 5 μm.

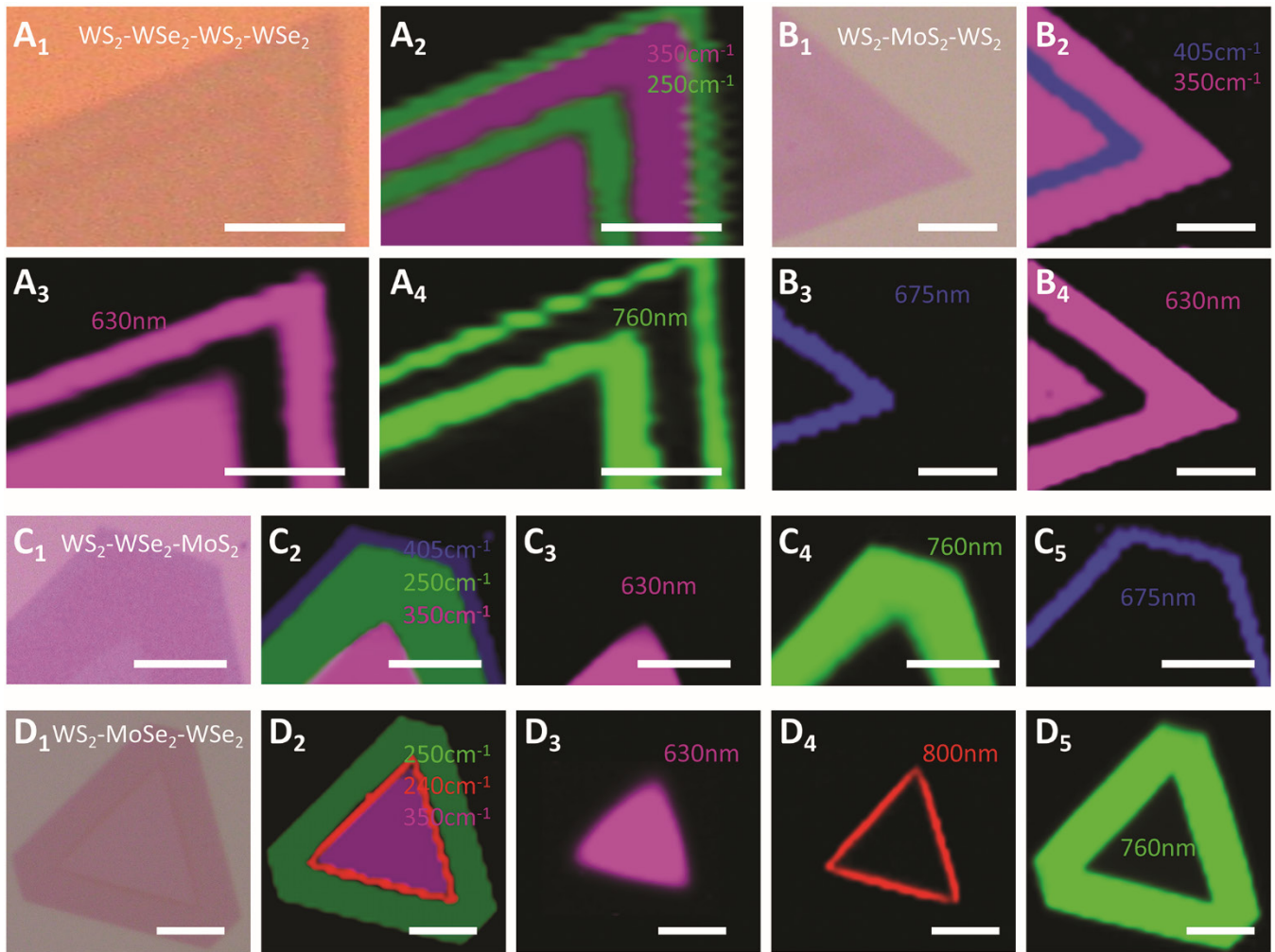


Fig. 3. Raman and photoluminescence characterizations of 2D superlattices and multiheterostructures. (A₁) Optical microscope image of WS₂-WSe₂-WS₂-WSe₂ superlattice on SiO₂/Si substrate. (A₂) Raman mapping image at 250 cm⁻¹ and 350 cm⁻¹ show clearly the WS₂-WSe₂ superlattice structure. (A₃-A₄) PL mapping images at 630 nm and 760 nm further confirm the WS₂-WSe₂ lateral superlattice structure. (B₁-B₄) Optical microscope image, Raman mapping and PL mapping images of the WS₂-MoS₂-WS₂ multiheterostructure on SiO₂/Si. Raman mapping at 405 cm⁻¹ and 350 cm⁻¹ show clearly the formation of WS₂-MoS₂-WS₂ multiheterostructure, which is confirmed by PL mapping images at 675 nm and 630 nm. (C₁-C₅) Optical microscope image, Raman mapping and PL mapping of the WS₂-WSe₂-MoS₂ multiheterostructure on SiO₂/Si. Raman mapping at 405 cm⁻¹, 250 cm⁻¹ and 350 cm⁻¹ show clearly the formation of WS₂-MoS₂-WS₂ multiheterostructure, which is confirmed by PL mapping images at 630 nm, 760 nm and 675 nm. (D₁-D₅) Optical microscope image, Raman mapping and PL mapping of the WS₂-MoSe₂-WSe₂ multiheterostructure on SiO₂/Si. Raman mapping at 250 cm⁻¹, 240 cm⁻¹ and 350 cm⁻¹ show clearly the formation of WS₂-MoS₂-WS₂ multiheterostructure, which is confirmed by PL mapping images at 630 nm, 800 nm and 760 nm. All scale bars correspond to 5 μm.

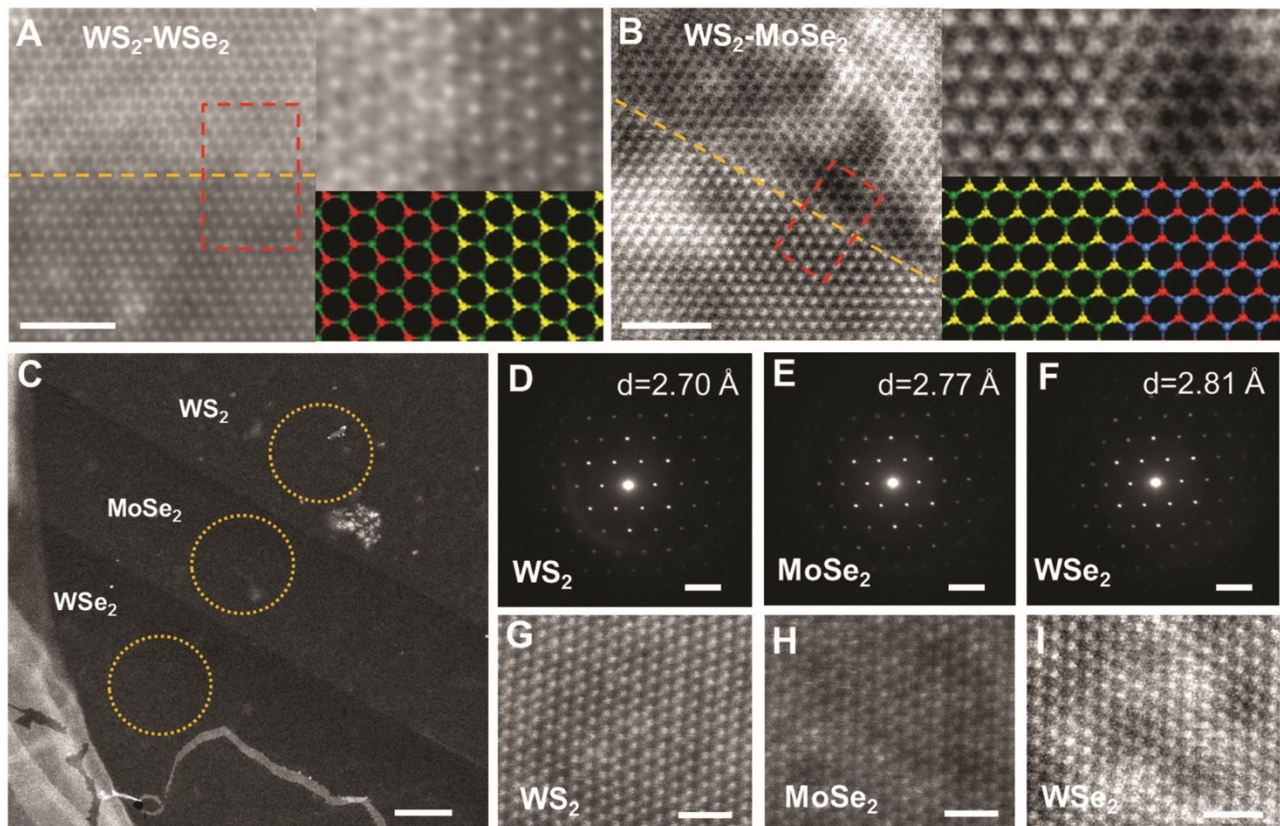


Fig. 4. Atomic structure of the lateral heterostructures and multiheterostructures. (A) Atomic-resolution Z-contrast STEM image taken from the $\text{WS}_2\text{-WSe}_2$ lateral heterostructure (left); Magnified STEM image of the doted red rectangle region (top right) and the corresponding atomic model (“interline”). Scale bar, 2 nm. (B) Atomic-resolution Z-contrast STEM image taken from the $\text{WS}_2\text{-MoSe}_2$ lateral heterostructure (left); Magnified STEM image of the doted red rectangle region (top right) and the corresponding atomic model (bottom right); The orange dashed lines highlight the atomically sharp “interline”. Scale bar, 2 nm. (C) Low-magnification Z-contrast image of the lateral $\text{WS}_2\text{-MoSe}_2\text{-WSe}_2$ multiheterostructure. Scale bar, 100 nm. (D, E, F) Electron diffraction patterns taken from the yellow doted circles in (C), corresponding to WS_2 region (D), MoSe_2 region (E) and WSe_2 region (F). Scale bar, 5 nm^{-1} . (G, H, I) Atomic-resolution STEM image taken from the WS_2 region (G), MoSe_2 region (H) and WSe_2 region (I). Scale bar, 1 nm.